



**HAL**  
open science

## Evaluation of the electrocatalytic properties of Tungsten electrode towards hydrogen evolution reaction in acidic solutions

Ghada Abd El-Hafez, Nady Mahmoud, Alain Walcarius, Amany Fekry

### ► To cite this version:

Ghada Abd El-Hafez, Nady Mahmoud, Alain Walcarius, Amany Fekry. Evaluation of the electrocatalytic properties of Tungsten electrode towards hydrogen evolution reaction in acidic solutions. *International Journal of Hydrogen Energy*, 2019, 44 (31), pp.16487-16496. 10.1016/j.ijhydene.2019.04.223 . hal-02324670

**HAL Id: hal-02324670**

**<https://hal.science/hal-02324670>**

Submitted on 26 Nov 2020

**HAL** is a multi-disciplinary open access archive for the deposit and dissemination of scientific research documents, whether they are published or not. The documents may come from teaching and research institutions in France or abroad, or from public or private research centers.

L'archive ouverte pluridisciplinaire **HAL**, est destinée au dépôt et à la diffusion de documents scientifiques de niveau recherche, publiés ou non, émanant des établissements d'enseignement et de recherche français ou étrangers, des laboratoires publics ou privés.

## **Evaluation of the electrocatalytic properties of Tungsten electrode towards hydrogen evolution reaction in acidic solutions**

Ghada M. Abd El-Hafez<sup>a</sup>, Nady H. Mahmoud<sup>a</sup>, Alain Walcarius<sup>b</sup>, Amany M. Fekry<sup>c\*</sup>

<sup>a</sup>*Chemistry Department, Faculty of Science, Fayoum University, Fayoum, Egypt*

<sup>b</sup>*CNRS-Université de Lorraine, LCPME UMR 7564, 405 Rue de Vandoeuvre, 54600 Villers-lès-Nancy, France*

<sup>c</sup>*Chemistry Department, Faculty of Science, Cairo University, 12 613 Giza- Egypt*

Corresponding author:

Name: Amany M. Fekry

Address: Chemistry Department, Faculty of Science, Cairo University, Giza-12613, Egypt

Tel: 202 0101545331

E-mail: amany.m.fekry@gmail.com

## **Abstract**

Hydrogen has concerned interest universally as an environmentally nontoxic and renewable fuel. Electrocatalytic hydrogen evolution reaction (HER) is one of the utmost favorable methods for hydrogen creation on a vast scale; however, the high cost of Pt-based supplies, which demonstrate the highest activity for HER, forced investigators to look for cheaper electro-catalysts. Tungsten has been considered as an effective, active and low cost electrocatalyst for the hydrogen evolution reaction, mostly in alkaline media, and we have investigated here its behavior in acid electrolytes. HER has been studied utilizing linear polarization technique and electrochemical impedance spectroscopy (EIS). It happens on W at rather low overpotential ( $-0.32$  V vs. NHE at  $10 \text{ mA cm}^{-2}$ , in  $0.5 \text{ M H}_2\text{SO}_4$ ), yet more cathodic than the widely used Pt/C catalyst, but not so far from more sophisticated systems developed recently. The effect of acid concentration on the HER rate and the electrode stability was investigated. Cathodic transfer coefficient and exchange current density were calculated for the HER from Tafel curves obtained in  $\text{H}_2\text{SO}_4$  solution at concentrations ranging from  $0.1$  to  $3.0 \text{ M}$ . EIS experiments were performed under both open circuit and/or cathodic polarization. It was found that the hydrogen evolution rate is relatively high under low overpotential, confirming that W is a possible applicant to substitute more expensive electrocatalysts usually used for the HER under acidic conditions. The process is economic and appropriate with no need for specific treatments, as supported by additional X-ray diffraction (XRD) and X-ray photoelectron spectroscopy (XPS) characterization of the tungsten electrode surface.

**Keywords:** Tungsten electrode; HER; Electrochemical activity; EIS.

## 1. Introduction

Hydrogen production from water electrolysis is a significant work owing to its importance as an alternative to hydrogen energy manufacturing field [1-3]. “Hydrogen economy” is a possible substitute to energy systems using fossil derived fuels, either for its useful environmental influence or as a substitute for rapidly exhausting fossil fuels [4,5]. HER has been studied on different electrode materials with the goal to find more efficient conditions for H<sub>2</sub> production. The active materials for HER should be of large active surface area, highly intrinsic electrocatalytic activity, stable and of low cost [4,6].

It is well recognized that noble metals like platinum, Pt, and palladium, Pd (especially Pt/C and Pd/C) have high efficient catalytic performance for the H<sub>2</sub> production, good chemical stability, large surface area with low overpotential in acid media [7]. However, their high price reduces their utilization for industrial applications [8, 9]. Therefore, much effort has been exhausted to find cost-effective, earth-abundant metal based compounds as a highly efficient HER catalyst [10].

Recently, non-precious metals like Ni [11], Co [12], W [13] or Mo [14], and/or non-noble metal-based materials, such as transition metal sulfides, nitrides, phosphides, carbides and carbonaceous materials, which have been stated as efficient HER catalysts replacing noble metal catalysts [15-17]. This is not only due to their chemical stability, but also because of their low cost and low HER overpotential [13,14]. In the tungsten family, more sophisticated W-based systems have been also reported for HER, including for instance tungsten carbide, tungsten oxide, tungsten sulfide or phosphide, tungsten-based alloys, or their multicomponent composites [18-30]. Note that tungsten oxide can be also used as

electrocatalyst for oxygen reduction [28]. Finally, one noticed also recent efforts directed towards the photocatalytic hydrogen generation using tungsten-based (nano) materials [31-39].

W was utilized successfully to produce H<sub>2</sub> from KOH solutions at a reasonable rate and for a relatively long time [13,40]. This is due to its superior electronic conductivity [41] that makes it significant candidate for electrocatalytic HER. The disadvantages of H<sub>2</sub>O alkaline electrolysis processes are mainly related to their low efficiency and high energy consumption [42-43].

Hence, W metal is inspected as a catalyst for the HER in this work in acid solution which provides a potential alternative to this issue. It is aimed to utilize it as an effective cathode for hydrogen evolution at low hydrogen overpotential in H<sub>2</sub>SO<sub>4</sub> solution. This suggestion was done especially on tungsten owing to its low cost, superior electronic properties and easily available. The electrochemical and catalytic characteristics of this electrode were investigated here on the basis of potentiometry and linear scan voltammetry (LSV) measurements as well as electrochemical impedance spectroscopy (EIS). Also, composition and morphological or structural properties have been included on the basis of SEM, EDX, XRD and XPS measurements.

## **2. Experimental**

The W rod (Sigma Aldrich of cross-section area of 0.2 cm<sup>2</sup>) was embedded in epoxy resin and then polished using successive grades of emery papers down to 2000 grit then washed with triple distilled water and transferred quickly to the electrolytic cell. The W working electrode was held using a PTFE holder. Its electrochemical response was evaluated in H<sub>2</sub>SO<sub>4</sub> medium (Sigma Aldrich) using

the Voltalab PGZ 100 workstation, most often with a three-electrode cell as stated previously in Badawy et al. [13] work. Triple distilled water was used.

The open circuit potential, OCP, was recorded for 1 h and all potential values are referred to the saturated calomel reference electrode (SCE, +0.241 V vs. NHE). All experiments were conducted at room temperature ( $25 \pm 1$  °C). Linear sweep voltammetry was performed at a scan rate of  $5 \text{ mV s}^{-1}$ . EIS tests were performed at OCP potential and at different overpotentials in the  $\text{H}_2$  evolution region with a 10 mV amplitude at frequency ranging from 1mHz to 100 kHz. The polarization and EIS tests were repeated three times. Pt electrode was used for comparison purposes.

Surface morphology and characterization was achieved utilizing the scanning electron microscope (SEM) (Model Quanta 250 Field Emission Gun) coupled with energy dispersive x-ray (EDX) Unit (FEI Company, Netherlands). XPS was collected on K-ALPHA (Thermo Fisher Scientific, USA) with monochromatic X-ray Al K-alpha radiation -10 to 1350 eV spot size 400 micro m at pressure  $10^{-9}$  mbar with full spectrum pass energy 200 eV and at narrow spectrum 50 eV. XRD instrument was ... Surface roughness was measured using the Nanosurf C3000 atomic force microscopy (AFM) apparatus.

### **3. Results and discussion**

#### ***3.1. Preliminary characterization of W electrodes***

The polished W rod electrode exhibited a flat surface (its roughness has been estimated from AFM imaging at about 45 nm), yet with noticeable polishing striations (see SEM micrograph on Fig. 1A), without any other detectable elements (as pointed out from EDX analysis, see Fig. 1B). XPS examination of its surface state (see the narrow scan corresponding to the W region on Fig. 1C)

reveals the presence of two main contributions of W(*4f*) at binding energies of respectively 31.3 and 33.5 eV, which are characteristics of metallic W<sup>0</sup>, and two small peaks located at 35.6 and 37.8 eV generally attributed to tungsten oxidized to its hexavalent state (WO<sub>3</sub>) [44-46]. The small amount of oxidized tungsten was even less after contacting a 0.5 M H<sub>2</sub>SO<sub>4</sub> solution (i.e., the medium in which most of electrochemical measurements will be performed, as described below), which should be due to some wet etching of WO<sub>3</sub> likely to occur in very acidic medium [46,47]. The residual WO<sub>3</sub> signature might be also due to the fact that the W sample was briefly exposed to air prior to XPS analysis, and might therefore not reflect exactly the surface state of the electrode in the electrolyte medium (as otherwise reported for air-sensitive materials [48]).

Both crude W electrode and W electrode treated with 0.5 M H<sub>2</sub>SO<sub>4</sub> have been characterized by XRD. The results (Fig. 2) indicate the expected body-centered cubic phase characteristic of W [49]. The same diffraction lines were observed for both crude and treated electrodes, with the typical reflections shown as (002) , (110), (200), (211) and (220), respectively located at 2 $\theta$  values of 29°, 40°, 58°, 73° and 87°. No noticeable difference can be seen after W treatment in 0.5 M H<sub>2</sub>SO<sub>4</sub>, and no crystalline WO<sub>3</sub> can be detected, suggesting that the small amount of oxide evidenced from XPS is either too low to be detected by XRD or amorphous.

### ***3.2. Open circuit potential***

The open-circuit potentials,  $E_{OCP}$ , of W (Fig. 3a) were monitored over 1 h in aerated H<sub>2</sub>SO<sub>4</sub> solution of various concentrations.  $E_{OCP}$  was reached in ~ 30 minutes at all acid concentrations, It shifted positively at first few minutes and then a gradual increase of potential with time until a steady state value is obtained (the relatively steady values are in the range of 0 to 0.50 mV). This means a

passivation and healing of W in aqueous media even with using a high acid concentration. By increasing the H<sub>2</sub>SO<sub>4</sub> concentration from 0.1-0.5 M, there is no appreciable change in the steady state potential,  $E_{ss}$ . At higher concentration of H<sub>2</sub>SO<sub>4</sub> (> 0.5 M), the  $E_{OCP}$  of the W electrode shifts toward more positive values indicating healing (*cf.* Fig. 3a). For comparison, the  $E_{OCP}$  for Pt in 0.5 M H<sub>2</sub>SO<sub>4</sub> solution was also outlined and the results of both Pt and W are set in Fig. 3b. The results indicate much more negative steady-state potential for W compared to Pt.

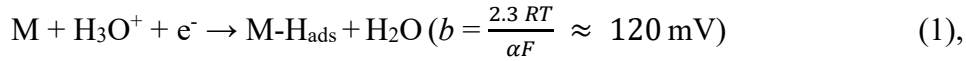
### ***3.3. Electrocatalytic evolution of hydrogen on W electrode***

The HER electrocatalytic activity for W electrode was estimated by the cathodic current-potential curves in different H<sub>2</sub>SO<sub>4</sub> acid concentrations (Fig. 4a) and examined in comparison with commercial Pt electrode. The increase of H<sub>2</sub>SO<sub>4</sub> concentration from 0.1 to 3.0 M resulted in different current densities related to the HER increasing from 95 to 592 mA cm<sup>-2</sup> at -1.0 V and from 182 to 1470 mA cm<sup>-2</sup> at -1.5 V. This means that the H<sub>2</sub> production can be controlled by the electrolyte concentration. Fig. 4b illustrates the hydrogen evolution behavior of W, in comparison to Pt in 0.5 M H<sub>2</sub>SO<sub>4</sub> solution, where the Pt catalyst exhibits the highest HER catalytic activity in the same solution, larger than that recorded on W electrode. These values are estimated from Fig. 4b, after enlargement of the current scale at 10 mA cm<sup>-2</sup> are -0.32 V and -0.08 V vs. NHE (in 0.5 M H<sub>2</sub>SO<sub>4</sub>), respectively, for W and Pt electrodes. The steady state potentials of Pt and W are 485 and -2 mV, respectively, (*cf.* Fig. 3b). The potential at which H<sub>2</sub> starts to evolve in the same solution on the two different electrodes is -310 and -596 mV for Pt and W, respectively (*cf.* Fig. 4b). Thus, the potential jump for HER on W amounts to -594 mV whereas that on Pt is -795 mV. So, W is an effective catalyst for H<sub>2</sub> production in H<sub>2</sub>SO<sub>4</sub> solutions. To compare between W and Pt according to

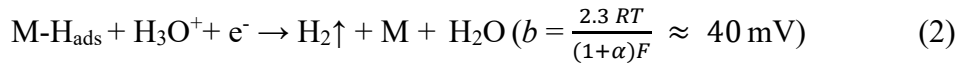
HER rate using similar polarization circumstances, the current density on W at -1.0 V from the steady-state potential amounts to 210 mA cm<sup>-2</sup>, i.e. only twice as less than on Pt (410 mA cm<sup>-2</sup>). The presented data were extracted from Fig. 4b at a concentration of 0.5 M H<sub>2</sub>SO<sub>4</sub> only. It was found that the hydrogen evolution rate is relatively high under low overpotential (-1 V). This confirms well confirming that W is a possible applicant as low cost electrocatalyst for the HER under acidic conditions. At higher concentration the rate of hydrogen evolution on W will be higher (*cf.* Fig. 4a). It means that even for practical applications when one needs to work in higher acid concentrations, W can act effectively as a catalyst for the HER in acidic electrolytes, yet achieving 50% of the performance in terms of current density when compared to Pt electrode. A more detailed comparison to other electrocatalysts investigated in the past few years (Table 1) shows that the overpotential values for W from the present study remains quite high, but not that much in comparison to other systems [50-87] that are often more sophisticated in terms of composition, (nano)structure or preparation methods, than a simple W rod as used here.

Fig. 5 presents the polarization scans of the HER on W electrode at different H<sub>2</sub>SO<sub>4</sub> concentrations fitted well with the Tafel equation [13]. The kinetic parameters were derived by the extrapolation method and are summarized in Table 2. The slope of the cathodic Tafel line,  $b$ , is given by:  $b=2.3RT/(1-\alpha)F$ , where it is inversely proportional to the cathodic transfer coefficient,  $(1-\alpha)$ . The exchange current density,  $i_0$ , is obtained from the intersection of Tafel lines. Generally, to convert H<sup>+</sup> protons to H<sub>2</sub> in acidic electrolytes, three elementary reaction steps are involved [88,89], as follow.

A primary discharge step (Volmer reaction):



An electrochemical-desorption step (Heyrowsky reaction):



and A recombination step (Tafel reaction):



Molecular  $\text{H}_2$  can be produced when reaction (1) is combined with reaction (2), or reaction (3). For materials that are good catalysts toward  $\text{H}_2$  production (HER), the Tafel reaction is the rate-determining step (*rds*) at low overpotentials, while at higher overpotentials, the Heyrowsky reaction becomes the *rds* [90]. The right reaction mechanism can't be simply known. As example, the Tafel slope for the HER on the Pt(110) was 28 mV/dec, indicating the reaction pathway to the Tafel-Volmer mechanism [91]. By knowing the evaluated values, we can assume that the route for HER on W ( $b = 25 \text{ mV dec}^{-1}$  cf. Table 1) should follow Volmer–Tafel steps, where Tafel reaction is the *rds*. It is also evaluated that the exchange current density increases with the  $\text{H}_2\text{SO}_4$  concentration. To know the actual meaning of the Tafel slope, the right value of the transfer coefficient  $\alpha$  should be known. The transfer coefficient for the HER is given to be between 0 and 1 [92]. The cathodic transfer coefficient decrease by a small value with increasing the  $\text{H}^+$  concentrations with an increase of exchange current density  $i_0$ , leading to an overall effect of HER enhancement [93]. Comparison to other HER catalysts indicates that Tafel slope achieved here with W electrode is amongst the smallest values reported to date for other electrode materials (Table 1).

### 3.4. EIS investigations of W electrode.

Metallic catalysts are likely to be corroded, inducing a decrease in its performance when utilized in industrial applications (activity and lifetime drops). Hence, EIS is an appropriate technique to characterize such behavior [94-99]. The Bode plots of W electrode after 1 h immersion in an aerated solution of different H<sub>2</sub>SO<sub>4</sub> concentrations were given in Fig. 6. They show a broad two time constants with a maximum phase angle of ~ 90° demonstrating that the corrosion reaction is mostly controlled by a charge transfer process. The phase diagram shape or phase angle maximum does not vary with the H<sub>2</sub>SO<sub>4</sub> concentration [99,100] ensuring the same reaction mechanism (Fig. 6). The data are fitted well utilizing an equivalent circuit model constituting a solution resistance,  $R_s$  in series with a two parallel combinations consisting of a resistor representing the charge transfer resistance of outer and inner layer,  $R_1$ ,  $R_2$ , respectively, and a constant phase element (CPE),  $CPE_1$ ,  $CPE_2$ , respectively, representing the double layer capacitance of the outer and inner layer (*cf.* Fig. 6 (inset)). The CPE is introduced to account for the non-ideality of the surface [101-103] including  $\alpha$  as an empirical parameter ( $0 \leq \alpha \leq 1$ ) and  $f$  as the frequency in Hz [104,105]. The experimental results were fitted to the circuit inset in Fig. 6 and the calculated parameters are given in Table 3. The total charge transfer resistance ( $R_T$ ) (Table 3) was found to be increased with increasing the concentration of H<sub>2</sub>SO<sub>4</sub> indicating a higher stability of W electrode at higher acidic solutions due to the formation of less soluble heteropolytungstates [100].

Fig. 7 presents the Bode and Nyquist plots of the W catalyst in H<sub>2</sub>SO<sub>4</sub> solutions at various concentrations, as polarized cathodically at a potential of -750 mV, where the HER is taking place at a measurable rate. Generally, the total

impedance,  $Z$ , under cathodic polarization, is lower (cf. Fig. 7a) owing to the activation of the W surface due to the HER. The  $\Theta_{max}$  value shifts toward lower values and the impedance,  $Z$ , value decreases in more concentrated  $H_2SO_4$  solutions, indicating an increase in the rate of  $H_2$  generation (HER). There is no broadening of phase diagram meaning that the rate of hydrogen production is appreciably high. Only one depressed semicircle was observed in Nyquist plot for W catalyst at all  $H_2SO_4$  concentrations (cf. Fig. 7b), which becomes smaller in more concentrated  $H_2SO_4$  due to the fact that the adsorption process is facilitated and the charge transfer process controls the mechanism as the concentration increases. The data can be adjusted utilizing the simple Randles model (Fig. 7b) and fitting values [106-110] are presented in Table 4. The charge-transfer resistance decreases as the acid concentrations increases. This confirms well the increase in the current density, i.e. the increase in HER rate. Fig. 8 presents the Bode and Nyquist plots performed after different intervals of electrode immersion in 0.5 M  $H_2SO_4$  at a cathodic potential of -750 mV.  $R_T$  increases due to a progressive adsorption of  $H^+$  on the electrode surface [7] as given in Table 5. The resistance of the adsorbed layer increases with increasing immersion time indicating increased adsorption of hydrogen on the electrode surface [111].

#### **4. Conclusions**

This work has investigated the electrocatalytic properties of tungsten electrode in 0.5 M  $H_2SO_4$  for hydrogen evolution reactions. Polarization and impedance results have shown that the hydrogen production occurs at a reasonable overpotential on W compared to other HER catalysts, yet more cathodic than the most efficient used to date (i.e., Pt/C or novel nanostructured catalysts), however, from cost

comparison W is better economically. Tungsten catalyst exhibited high HER activity with an overpotential of -0.32 V vs. NHE (at 10 mA cm<sup>-2</sup>, in 0.5 M H<sub>2</sub>SO<sub>4</sub>), large cathodic current, and a Tafel slope as small as 25 mV/decade, which makes them perspective for application in acidic electrolyzers for hydrogen production.

## References

1. Mizuno T, Enyo M, Sorption of hydrogen on and in hydrogen absorbing metals in electrochemical environment. In: Modern aspects of electrochemistry, New York: Plenum 1996;35:415.
2. Viswanathan B. In: Viswanathan B, editor. Catalysis. New Delhi, India: Narosa Publishing House;2002:390.
3. Losiewicz B, Budniok A, Rowinski E, Lagiewka E, Lasia A. The structure, morphology and electrochemical impedance study of the hydrogen evolution reaction on the modified nickel electrodes. *Int J Hydrogen Energy* 2004;29:145–157.
4. Crabtree GW, Dresselhaus MS, Buchanan MV. The hydrogen economy. *Phys Today* 2004;57:39-45.
5. Tseng P, Lee J, Friley P. A hydrogen economy: opportunities and challenges. *Energy* 2005;30:2703-2720.
6. Navarro-Flores E, Omanovic S. Hydrogen evolution on nickel incorporated in three-dimensional conducting polymer layers. *Mol Catal A: Chem* 2005;242:182-194.
7. Sarkar S, Peter S. An overview on Pd-based electrocatalysts for the hydrogen evolution reaction, *Inorg. Chem. Front.*, 2018;5:2060-2080.
8. Huang H, Zhang X, Zhang Y, Huang B, Cai J, Lin S, Facile synthesis of laminated porous WS<sub>2</sub>/C composite and its electrocatalysis for oxygen reduction reaction. *Int J Hydrogen Energy* 2018;43:8290-8297.
9. Grigoriev S, Porembsky V, Fateev V. Pure hydrogen production by PEM electrolysis for hydrogen energy. *Int J Hydrogen Energy* 2006;31:171-175.

10. Imran M, Yousaf A, Zaidi S, Fernandez C. Tungsten-molybdenum oxide nanowires/reduced graphene oxide nanocomposite with enhanced and durable performance for electrocatalytic hydrogen evolution reaction, *Int J Hydrogen Energy* 2017;42:8130-8138.
11. Popczun EJ, McKone JR, Read CG, Biacchi AJ, Wiltrout AM, Lewis NS, Schaak RE. Nanostructured nickel phosphide as an electrocatalyst for the hydrogen evolution reaction. *J Am Chem Soc* 2013;135:9267-9270.
12. Zhong H, Campos-Roldan CA, Zhao Y, Zhang S, Feng Y, Alonso-Vante N. Recent advances of cobalt-based electrocatalysts for oxygen electrode reactions and hydrogen evolution reaction. *Catalysts* 2018;8:559.
13. Badawy WA, Abd El-Hafez GM, Nady H. Electrochemical performance of tungsten electrode as cathode for hydrogen evolution in alkaline solutions. *Int J Hydrogen Energy* 2015;40:6276–6282.
14. Badawy WA, Feky HE, Helal NH, Mohammed HH. Hydrogen production on molybdenum in H<sub>2</sub>SO<sub>4</sub> solutions. *J Power Sources* 2014;271:480-488.
15. Shi, Y.; Zhang, B. Recent advances in transition metal phosphide nanomaterials: synthesis and applications in hydrogen evolution reaction. *Chem Soc Rev* 2016;45:1529-1541.
16. Liu, Y.; Li, Y.; Kang, H.; Jin, T.; Jiao, L. Design, synthesis, and energy-related applications of metal sulfides, *Mater Horizons* 2016;3:402-421.
17. Li, X.; Hao, X.; Abudula, A.; Guan, G. Nanostructured catalysts for electrochemical water splitting: current state and prospects. *J Mater Chem A* 2016;4:11973-12000.

18. Zhang Y, Bilal HK, Podlaha E. Enhancing the hydrogen evolution reaction with Ni-W-TiO<sub>2</sub> composites *Electrochem Commun* 2018;96:108-112.
19. Nayak AK, Verma M, Sohn Y, Deshpande PA, Pradhan D. Highly Active Tungsten Oxide Nanoplate Electrocatalysts for the Hydrogen Evolution Reaction in Acidic and Near Neutral Electrolytes. *ACS Omega* 2017;2:7039-7047.
20. Li YH, Liu PF, Pan LF, Wang HF, Yang ZZ, Zheng LR, Hu P, Zhao HJ, Gu L, Yang HG. Local atomic structure modulations activate metal oxide as electrocatalyst for hydrogen evolution in acidic water. *Nature Commun* 2015;6:8064.
21. Fei H, Yang Y, Fan X, Wang G, Ruan G, Tour JM. Tungsten-based porous thin-films for electrocatalytic hydrogen generation. *J Mater Chem A* 2015;3:5798-5804.
22. Park I, Kim W, Kim E, Bae S, Kim J, Shin H. Electrochemical Reactivity of Chemically Roughened Tungsten Electrodes. *Asian J Chem* 2013;25:7037-7040.
23. Struck B, Neumeister H., Naoumidis A., Tungsten carbide cathodes for hydrogen production in acidic electrolytes, *Int J Hydrogen Energy* 1986;11:541-548.
24. Zóltovski P., Hydrogen evolution reaction on smooth tungsten carbide electrodes, *Electrochim Acta* 1980;25:1547-1554.
25. Wondimu T., Chen G., Kabtamu D., Chen H., Bayeh A., Huang H., Wang C., Highly efficient and durable phosphine reduced iron-doped tungsten oxide/reduced graphene oxide nanocomposites for the hydrogen evolution reaction, *Int J Hydrogen Energy* 2018;43:6481-6490.

26. Abbas S., Wu J., Huang Y., Babu D., Anandhababu G., Ghausi M., Wu M., Wang Y., Novel strongly coupled tungsten-carbon-nitrogen complex for efficient hydrogen evolution reaction, *Int J Hydrogen Energy* 2018;43:16-23.
27. Han N., Yang K., Lu Z., Li Y., Xu W., Gao T., Cai Z., Zhang Y., Batista V., Liu W., Sun X., Nitrogen-doped tungsten carbide nanoarray as an efficient bifunctional electrocatalyst for water splitting in acid, *Nature Commun* 2018;9:924.
28. Nsanzimana J., Peng Y., Miao M., Reddu V., Zhang W., Wang H., Xia B., Wang X., An Earth-Abundant Tungsten–Nickel Alloy Electrocatalyst for Superior Hydrogen Evolution, *ACS Appl Nano Mater* 2018;1:1228–1235.
29. McEnaney J., Chance Crompton J., Callejas J., Popczun E., Read C., Lewis N., Schaak R., Electrocatalytic hydrogen evolution using amorphous tungsten phosphide nanoparticles, *Chem Commun* 2014;50:11026-11028.
30. Wu L., Pu Z., Tu Z., Amiin I., Liu S., Wang P., Mu S., Integrated design and construction of WP/W nanorod array electrodes toward efficient hydrogen evolution reaction, *Chem Eng J* 2017;327:705-712.
31. Liu Y., Shrestha S., Mustain W, Synthesis of Nanosize Tungsten Oxide and Its Evaluation as an Electrocatalyst Support for Oxygen Reduction in Acid *Media*, *ACS Catal* 2012;2:456–463.
32. Tahir M., Nabi G, Rafique M, Khalid N. Nanostructured-based WO<sub>3</sub> photocatalysts: recent development, activity enhancement, perspectives and applications for wastewater treatment. *Int J Environ Sci Technol* 2017;14:2519–2542.

33. Tahir M, Sagir M, Shahzad K. Removal of acetylsalicylate and methyltheobromine from aqueous environment using nano-photocatalyst  $\text{WO}_3\text{-TiO}_2@g\text{-C}_3\text{N}_4$  composite, *J Hazardous Mater* 2019;363:205-213.
34. Tahir M, Sagir M. Carbon nanodots and rare metals (RM = La, Gd, Er) doped tungsten oxide nanostructures for photocatalytic dyes degradation and hydrogen production, *Sep Purif Technol* 2019;209:94-102.
35. Tahir M. Construction of  $\text{MoS}_2/\text{CND-WO}_3$  Ternary Composite for Photocatalytic Hydrogen Evolution, *J Inorg Organomet Polym Mater* 2018;28:2160-2168.
36. Tahir M, Nabi G, Khalid N. Enhanced photocatalytic performance of visible-light active graphene- $\text{WO}_3$  nanostructures for hydrogen production, *Mater Sci Semicond Process* 2018;84:36-41.
37. Tahir M, Nabi G, T.Iqbal T, Sagir M, Rafique M. Role of  $\text{MoSe}_2$  on nanostructures  $\text{WO}_3\text{-CNT}$  performance for photocatalytic hydrogen evolution. *Ceram Int* 2018;44:6686-6690.
38. Tahir M, Nabi G, Khalid N, Rafique M. Role of europium on  $\text{WO}_3$  performance under visible-light for photocatalytic activity. *Ceram Int* 2018;44:5705-5709.
39. Tahir M, .Asiri A, Nabi G, Rafique M, Sagir M. Fabrication of heterogeneous photocatalysts for insight role of carbon nanofibre in hierarchical  $\text{WO}_3/\text{MoSe}_2$  composite for enhanced photocatalytic hydrogen generation. *Ceram Int* 2019;45:5547-5552.
40. Borresen B, Hagen G, Tunold R. Hydrogen evolution on  $\text{Ru}_x\text{Ti}_{1-x}\text{O}_2$  in 0.5 M  $\text{H}_2\text{SO}_4$ . *Electrochim Acta* 2000;47:1819–1827.

41. Liu C, Zhou J, Xiao Y, Yang L, Yang D, Zhou D, Structural and electrochemical studies of tungsten carbide/carbon composites for hydrogen evolution, *Int J Hydrogen Energy* 2017;42:29781-29790.
42. Tuvic T, Pasti I, Mentus SV, A rotating tungsten disc electrode in concentrated strong alkaline solutions: an electroanalytical aspect, *J Electroanal Chem* 2011;654:102-107.
43. Kelly EJ, Bronstein HR. Kinetics and Mechanism of the Hydrogen Evolution Reaction on Titanium in Acidic Media. *J Electrochem Soc* 1984;131:2232-2238.
44. Tamboli D, Seal S, Desai V, Maury A, Tamboli D, Seal S, Desai V, Maury A. Studies on passivation behavior of tungsten in application to chemical mechanical polishing. *J Vacuum Sci Technol* 1999;17:1168-1173.
45. Kamiura Y., Umezawa K, Teraoka Y, Yoshigoe A. Characterization of polycrystalline tungsten surfaces irradiated with nitrogen ions by X-ray photoelectron spectroscopy. *Mater Trans* 2016;57:1609-1614.
46. Votta A., Pipia F, Borsari S, Ravizza E, Elbaz A, Alessandri M, Bellandi E, Bresolin C. Influence of Wet Cleaning on Tungsten Deposited with Different Techniques, *Solid State Phenom* 2009, 145-146, 197-200.
47. Reichman B, Bard AJ. The Electrochromic Process at  $WO_3$  Electrodes Prepared by Vacuum Evaporation and Anodic Oxidation of W. *J Electrochem Soc* 1979;126:583-591.
48. Bogdanoff P, Harbauer K, Plate P, Höhn C, Rappich J, Wang B, Han X, van de Krol R, Fiechter S. Structural Transformation Identification of Sputtered Amorphous  $MoS_x$  as an Efficient Hydrogen-Evolving Catalyst during Electrochemical Activation. *ACS Catal* 2019;9:2368–2380.

49. Majumdar S, Kishor J, Paul B, Kain V, Dey GK. Demonstration of Production of Tungsten Metal Powder and its Consolidation into Shapes. BARC Newsletter 2016, pp. 30-33.
50. Chen, Z.; Cummins, D.; Reinecke, B. N.; Clark, E.; Sunkara, M. K.; Jaramillo, T. F. Core-shell MoO<sub>3</sub>-MoS<sub>2</sub> Nanowires for Hydrogen Evolution: A Functional Design for Electrocatalytic Materials. *Nano Lett* 2011;11:4168-4175.
51. Wang, T. Y.; Liu, L.; Zhu, Z. W.; Papakonstantinou, P.; Hu, J. B.; Li, M. Enhanced Electrocatalytic Activity for Hydrogen Evolution Reaction from Self-Assembled Monodispersed Molybdenum Sulfide Nanoparticles on an Au Electrode. *Energy Environ Sci* 2013;6: 625-633.
52. Xie, J.; Zhang, H.; Li, S.; Wang, R.; Sun, X.; Zhou, M.; Zhou, J.; Lou, X. W.; Xie, Y. Defect-Rich MoS<sub>2</sub> Ultrathin Nanosheets with Additional Active Edge Sites for Enhanced Electrocatalytic Hydrogen Evolution. *Adv Mater* 2013;25:5807-5813.
53. Popczun, E. J.; McKone, J. R.; Read, C. G.; Biacchi, A. J.; Wiltrout, A. M.; Lewis, N. S.; Schaak, R. E. Nanostructured Nickel Phosphide as an Electrocatalyst for the Hydrogen Evolution Reaction. *J Am Chem Soc* 2013;135:9267-9270.
54. Kong, D. S.; Cha, J. J.; Wang, H. T.; Lee, H. R.; Cui, Y. First-Row Transition Metal Dichalcogenide Catalysts for Hydrogen Evolution Reaction. *Energy Environ Sci* 2013;6:3553-3558.
55. Liu, Q.; Tian, J. Q.; Cui, W.; Jiang, P.; Cheng, N. Y.; Asiri, A. M.; Sun, X. P. Carbon Nanotubes Decorated with CoP Nanocrystals: A Highly Active

- Non-Noble-Metal Nanohybrid Electrocatalyst for Hydrogen Evolution. *Angew Chem Int Ed* 2014;53:6710-6714.
56. Fu, Q.; Yang, L.; Wang, W.; Han, A.; Huang, J.; Du, P.; Fan, Z.; Zhang, J.; Xiang, B. Synthesis and Enhanced Electrochemical Catalytic Performance of Monolayer  $WS_{2(1-x)}Se_{2x}$  with a Tunable Band Gap. *Adv Mater* 2015;27:4732-4738.
  57. Zou, M.; Zhang, J.; Zhu, H.; Du, M.; Wang, Q.; Zhang, M.; Zhang, X. A 3D Dendritic WSe<sub>2</sub> Catalyst Grown on Carbon Nanofiber Mats for Efficient Hydrogen Evolution. *J Mater Chem A* 2015;3:12149-12153.
  58. Wu, R.; Zhang, J.; Shi, Y.; Liu, D.; Zhang, B. Metallic WO<sub>2</sub>-Carbon Mesoporous Nanowires as Highly Efficient Electrocatalysts for Hydrogen Evolution Reaction. *J Am Chem Soc* 2015;137:6983-6986.
  59. Fan, X.; Zhou, H.; Guo, X. WC Nanocrystals Grown on Vertically Aligned Carbon Nanotubes: An Efficient and Stable Electrocatalyst for Hydrogen Evolution Reaction. *ACS Nano* 2015;9:5125-5134.
  60. Nayak, A. K.; Verma, M.; Sohn, Y.; Deshpande, P. A.; Pradhan, D. Highly Active Tungsten Oxide Nanoplate Electrocatalyst for Hydrogen Evolution Reaction in Acidic and Near Neutral Electrolytes. *ACS Omega* 2017;2:7039-7047.
  61. Zhu, Y.; Chen, G.; Xu, X.; Yang, G.; Liu, M.; Shao, Z. Enhancing Electrocatalytic Activity for Hydrogen Evolution by Strongly Coupled Molybdenum Nitride@Nitrogen-Doped Carbon Porous Nano-Octahedrons. *ACS Catal* 2017, 7, 3540-3547.
  62. Theerthagiri, J.; Sudha, R.; Premnath, K.; Arunachalam, Prabhakarn; Madhavan, J.; Al-Mayouf, A. M. Growth of Iron Diselenide Nanorods on

- Graphene Oxide Nanosheets as Advanced Electrocatalysts for Hydrogen Evolution Reaction. *Int J Hydrogen Energy* 2017, 42, 13020-13030.
63. Ren, W.; Zhang, H.; Cheng, C. Ultrafine Pt Nanoparticles Decorated MoS<sub>2</sub> Nanosheets with Significantly Improved Hydrogen Evolution Activity. *Electrochim Acta* 2017;241:316-322.
  64. Xu, X. Y.; Dong, X. F.; Bao, Z. J.; Wang, R.; Hu, J. G.; Zeng, H. B. Three Electron Channels Toward two Types of Active Sites in MoS<sub>2</sub>@Pt Nanosheets for Hydrogen Evolution. Novel Porous Tungsten Carbide Hybrid Nanowires on Carbon Cloth for High-Performance Hydrogen Evolution. *J Mater Chem A* 2017;5:22654-22661.
  65. Ren, B.; Li, D.; Jin, Q.; Cui, H.; Wang, C. Novel Porous Tungsten Carbide Hybrid Nanowires on Carbon Cloth for High-Performance Hydrogen Evolution. *J Mater Chem A* 2017;5:13196-13203.
  66. Kuang, P.; Tong, T.; Fan, K.; Yu, J. In Situ Fabrication of Ni-Mo Bimetal Sulfide Hybrid as an Efficient Electrocatalyst for Hydrogen Evolution over a Wide pH Range. *ACS Catal* 2017;7:6179-6187.
  67. Bhat, K. S.; Barshilia, H. C.; Nagaraja, H. S. Porous Nickel Telluride Nanostructures as Bifunctional Electrocatalyst Towards Hydrogen and Oxygen Evolution Reaction. *Int J Hydrogen Energy* 2017;42:24645-24655.
  68. Min, S.; Qin, J.; Hai, W.; Lei, Y.; Hou, J.; Wang, F. Electrochemical Growth of MoS<sub>x</sub> on Cu Foam: A Highly Active and Robust Three-Dimensional Cathode for Hydrogen Evolution. *Int J Hydrogen Energy* 2018;43:4978-4986.
  69. Zhang, Y.; Tan, J.; Wen, F.; Zhou, Z.; Zhu, M.; Yin, S.; Wang, H. Platinum Nanoparticles Deposited Nitrogen-Doped Carbon Nanofiber Derived from

- Bacterial Cellulose for Hydrogen Evolution Reaction. *Int J Hydrogen Energy* 2018;43:6167-6176.
70. Li, Y.; Niu, S.; Rakov, D.; Wang, Y.; Caban-Acevedo, M.; Zheng, S.; Song, B.; Xu, P. Metal organic framework-derived CoPS/N-doped carbon for efficient electrocatalytic Hydrogen Evolution. *Nanoscale* 2018;10: 7291-7297.
  71. Yu, S. H.; Chua, D. H. C. Toward High-Performance and Low-Cost Hydrogen Evolution Reaction Electrocatalysts: Nanostructuring Cobalt Phosphide (CoP) Particles on Carbon Fiber Paper. *ACS Appl Mater Interfaces* 2018;10:14777-14785.
  72. Mao, B.; Wang, B.; Yu, F.; Zhang, K.; Zhang, Z.; Hao, J.; Zhong, J.; Liu, Y.; Shi, W. Hierarchical MoS<sub>2</sub> Nanoflowers on Carbon Cloth as an Efficient Cathode Electrode for Hydrogen Evolution Under all pH Values. *Int J Hydrogen Energy* 2018;43:11038-11046.
  73. Zhang, M.; Hu, A.; Liu, Z.; Xu, Y.; Fan, B.; Tang, Q.; Zhang, S.; Deng, W.; Chen, X. Synergistic Effect of Three-Dimensional Cobalt Diselenide/Carbon Nanotube Arrays Composites for Enhanced Hydrogen Evolution Reaction. *Electrochim Acta* 2018;285:254-261.
  74. Sakamoto, R.; Shiotsuki, R.; Wada, K.; Fukui, N.; Maeda, H.; Komeda, J.; Sekine, R.; Harano, K.; Nishihara, H. A Pyrazine-Incorporated Graphdiyne Nanofilm as a Metal-Free Electrocatalyst for the Hydrogen Evolution Reaction. *J Mater Chem. A* 2018 ;6:22189-22194.
  75. Nsabimana, A.; Wu, F.; Lai, J.; Liu, Z.; Luque, R.; Xu, G. Simple Synthesis of Nitrogen-Doped Porous Carbon from Chinese Steamed Bread Flour and

- its Catalytic Application for Hydrogen Evolution Reaction. *Electrochim Acta* 2018;290:30-37.
76. Zhou, Y.; Yang, Y.; Wang, R.; Wang, X.; Zhang, X.; Qiang, L.; Wang, W.; Wang, Q.; Hu, Z. Rhombic Porous CoP<sub>2</sub> Nanowire Arrays Synthesized by Alkaline Etching as Highly Active Hydrogen Evolution Reaction Electrocatalysts. *J Mater Chem A* 2018;6:19038-19046.
77. Wang, C.; Shi, H.; Liu, H.; Fu, J.; Wei, D.; Zeng, W.; Wan, Q.; Zhang, G.; Duan, H. Quasi-Atomic-Scale Platinum Anchored on Porous Titanium Nitride Nanorod Arrays for Highly Efficient Hydrogen Evolution. *Electrochim Acta* 2018;292:727-735.
78. Li, S.; Zhang, L.; Lan, Y.; O'Halloran, K. P.; Ma, H.; Pang, H. Polyoxometalate-Encapsulated Twenty-Nuclear silver-Tetrazole Nanocage Frameworks as Highly Active Electrocatalysts for the Hydrogen Evolution Reaction. *Chem Commun* 2018;54:1964-1967.
79. Park, J.; Jin, H.; Lee, J.; Oh, A.; Kim, B.; Kim, J. H.; Baik, H.; Joo, S. H.; Lee, K. Highly Crystalline Pd<sub>13</sub>Cu<sub>3</sub>S<sub>7</sub> Nanoplates Prepared via Partial Cation Exchange of Cu<sub>1.81</sub>S Templates as an Efficient Electrocatalyst for the Hydrogen Evolution Reaction. *Chem Mater* 2018;30:6884-6892.
80. Ren, Q.; Jin, H.; Xu, X.; Liu, A.; Li, J.; Wang, J.; Wang, S. Hydrogen Evolution Reaction Catalyzed by Nickel/Nickel Phosphide Nanospheres Synthesized through Electrochemical Methods. *Electrochim Acta* 2019;298:229-236.
81. Sharma, M. D.; Mahala, C.; Basu, M. AgPd Alloy Nanoparticles Decorated MoS<sub>2</sub> 2D Nanosheets: Efficient Hydrogen Evolution Catalyst in Wide pH Condition. *ChemistrySelect* 2019;4:378-386.

82. Sun, J.; Ren, M.; Yu, L.; Yang, Z.; Xie, L.; Tian, F.; Yu, Y.; Ren, Z.; Chen, S.; Zhou, H. Highly Efficient Hydrogen Evolution from a Mesoporous Hybrid of Nickel Phosphide Nanoparticles Anchored on Cobalt Phosphosulfide/Phosphide Nanosheet Arrays. *Small* 2019;15:1804272.
83. Zheng, L.; Zheng, S.; Wei, H.; Du, L.; Zhu, Z.; Chen, J.; Yang, D. Palladium/Bismuth/Copper Hierarchical Nano-Architectures for Efficient Hydrogen Evolution and Stable Hydrogen Detection. *ACS Appl Mater Interfaces* 2019;11: 6248-6256.
84. Wei, Y.; He, W.; Sun, P.; Yin, J.; Deng, X.; Xu, X. Synthesis of Hollow Cu/Cu<sub>2</sub>O/Cu<sub>2</sub>S Nanotubes for Enhanced Electrocatalytic Hydrogen Evolution. *Appl Surf Sci* 2019;476:966-971.
85. Hu, Y.; Yu, B.; Li, W.; Ramadoss, M.; Chen, Y. W<sub>2</sub>C Nanodot-Decorated CNT Networks as a Highly Efficient and Stable Electrocatalyst for Hydrogen Evolution in Acidic and Alkaline Media. *Nanoscale* 2019;11:4876-4884.
86. Nguyen, V.-T.; Nguyen, N.-A.; Ali, Y.; Tran, Q. C.; Choi, H.-S. Graphene Dot Armored PtMo Nanosponge as a Highly Efficient and Stable Electrocatalyst for Hydrogen Evolution Reactions in both Acidic and Alkaline Media. *Carbon* 2019;146:116-124.
87. Karuppasamy, K.; Jothi, V. R.; Vikraman, D.; Prasanna, K.; Maiyalagan, T.; Sang, B.-I.; Yi, S.-C.; Kim, H.-S. Metal-Organic Framework Derived NiMo Polyhedron as an Efficient Hydrogen Evolution Reaction Electrocatalyst. *Appl Surf Sci* 2019;478:916-923.

88. Conway BE, Tilak BV. Behavior and Characterization of Kinetically Involved Chemisorbed Intermediates in Electrocatalysis of Gas Evolution Reactions. *Adv Catal* 1992;38:1–147.
89. Gileadi E. *Electrode Kinetics for Chemists, Chemical Engineers and Material Scientists* 1993;164, VCH, Weinheim, Germany.
90. Markovic NM, Grgur BN, Ross PN. Temperature-Dependent Hydrogen Electrochemistry on Platinum Low-Index Single-Crystal Surfaces in Acid Solutions. *J Phys Chem B* 1997;101:5405–5413.
91. Vielstich W, Lamm A, Gasteiger HA. *Handbook of fuel cells: fundamentals, technology, and applications*. Hoboken, N.J: Wiley, Chichester, England 2003.
92. Bockris J, Reddy A, Gamboa-Aldeco M. *Modern electrochemistry*. 2<sup>nd</sup> ed., New York: Kluwer Academic Publishers; 2002;1480.
93. Macdonald JR. *Impedance Spectroscopy*, John Wiley and Sons, New York, (Chapter 4) 1987.
94. Badawy WA, Al-Kharafi FM, El-Azab AS. Electrochemical behavior and corrosion inhibition of Al, Al-6061 and Al-Cu in neutral aqueous solutions. *Corros Sci* 1999;41:709-727.
95. Nady H, Negem M. Ni–Cu nano-crystalline alloys for efficient electrochemical hydrogen production in acid water. *RSC Adv* 2016;6:51111–51119.
96. Ismail KM, Fathi AM, Badawy WA. Effect of Nickel Content on the Corrosion and Passivation of Copper-Nickel Alloys in Sodium Sulfate Solutions. *Corrosion* 2004; 60:795-803.

97. Kucernak ARJ, Naranammalpuram Sundaram VN. Nickel phosphide: the effect of phosphorus content on hydrogen evolution activity and corrosion resistance in acidic medium. *J Mater Chem A* 2014;2:17435–17445.
98. Badawy WA, Hilal NH, El-Rabiee M, Nady H. Electrochemical behavior of Mg and some Mg alloys in aqueous solutions of different pH. *Electrochim Acta* 2010;55:1880-1887.
99. Badawy WA, Nady H, Negem M. Cathodic Hydrogen Evolution in Acidic Solutions Using Electrodeposited Nano-crystalline Ni-Co Cathodes. *Int J Hydrogen Energy* 2014; 39:10824-10832.
100. Lavrenko VO. Kinetics of electrochemical anodic oxidation of tungsten. *Zhur Fiz Khim* 19961;35:1095-1102.
101. Shehata M, Azab S, Fekry AM, Ameer MA. Nano-TiO<sub>2</sub> modified carbon paste sensor for electrochemical nicotine detection using anionic surfactant. *Biosens Bioelectron*, 2016;79:589-592.
102. Ahmed RA, Fekry AM, Farghali RA. A study of calcium carbonate/multiwalled-carbon nanotubes/chitosan composite coatings on Ti–6Al–4V alloy for orthopedic implants. *Appl Surf Sci* 2013;285B:309–316.
103. Fekry AM. A new simple electrochemical Moxifloxacin Hydrochloride sensor built on carbon paste modified with silver nanoparticles. *Biosens Bioelectron*, 2017;87:1065-1070.
104. Heakal F, Shehata O, Tantawy N, Fekry AM. Investigation on the corrosion and hydrogen evolution for AZ91D magnesium alloy in single and anion-containing oxalate solutions. *Int J Hydrogen Energy* 2012;37:84-94.

105. Fekry MA, Ghoneim AA, Ameer MA. Electrochemical impedance spectroscopy of chitosan coated magnesium alloys in a synthetic sweat medium. *Surf Coat Technol* 2014;38:126-132.
106. Abdelrahman, E. M., Abo-Ezz, E. R., Essa, K. S., El-Araby, T. M., Soliman, K. S. A least-squares variance analysis method for shape and depth estimation from gravity data. *J Geophys Eng* 2006;3:143-153.
107. Abdelrahman, E. M., Abo-Ezz, E. R., Essa, K. S. Parametric inversion of residual magnetic anomalies due to simple geometric bodies. *Exploration Geophys* 2012;43,178-189.
108. Essa, K. S., Mehane, S., Smith, P. A new inversion algorithm for estimating the best fitting parameters of some geometrically simple body from measured self-potential anomalies. *Exploration Geophys* 2008;39:155-163.
109. Abdelrahman, E. M., Abo-Ezz, E. R., Essa, K. S., El-Araby, T. M., Soliman, K. S. A new least-squares minimization approach to depth and shape determination from magnetic data. *Geophys Prospecting* 2007;55:433-446.
110. Abdelrahman, E. M., El-Araby, H. M., El-Araby, T. M., Essa, K. S. A least-squares minimization approach to depth determination from magnetic data. *Pure Appl Geophys* 2003;160:1259-1271.
111. Badawy WA, Ismail KM, Fathi AM. The influence of the Copper/Nickel Ratio on the Electrochemical Behavior of Cu-Ni Alloys in Acidic Sulfate Solutions. *J Alloy Compd* 2009;484:365-370.

### Figures captions:

**Fig. 1.** (A) SEM micrograph and (B) EDX spectrum corresponding to a freshly polished W electrode. (C) High resolution XPS spectra for W (4f) recorded with W electrode, respectively, before (C<sub>1</sub>) and after contacting a 0.5 M H<sub>2</sub>SO<sub>4</sub> solution (C<sub>2</sub>).

**Fig. 2.** XRD patterns for A) a crude W electrode (without polishing) and B) W electrode treated with 0.5 M H<sub>2</sub>SO<sub>4</sub> (with polishing).

**Fig. 3.** (a) Variation of the open circuit potential with time for W electrode immersed in H<sub>2</sub>SO<sub>4</sub> solutions of different concentrations at 25 °C. (b) Variation of the open-circuit potential with time for W and Pt electrodes in a stable natural aerated 0.5 M H<sub>2</sub>SO<sub>4</sub> solution.

**Fig. 4.** (a) Influence of H<sub>2</sub>SO<sub>4</sub> solution concentration on the catalytic activity of W electrode at 25 °C. (b) Cathodic polarization curves for HER on W and Pt in 0.5 M H<sub>2</sub>SO<sub>4</sub> at 25 °C.

**Fig. 5.** Cathodic Tafel lines for HER on W electrode immersed in aerated H<sub>2</sub>SO<sub>4</sub> solution of different concentrations at 25 °C.

**Fig. 6.** Bode plots for W electrode immersed in H<sub>2</sub>SO<sub>4</sub> solutions of different concentrations after 60 min of electrode immersion at 25 °C. (inset): Equivalent circuit model used in the impedance data fitting. Where  $R_s$ = solution resistance,  $R_p$ = polarization resistance,  $C_{dl}$ = double layer capacitance.

**Fig. 7.** (a) Bode plots for W electrode at  $E = -750$  mV vs SCE, for HER at different concentrations of H<sub>2</sub>SO<sub>4</sub> solutions at 25 °C. (b) Nyquist plots for W electrode at  $E = -750$  mV vs SCE, for HER at different concentrations of H<sub>2</sub>SO<sub>4</sub> solutions at 25 °C.

**Fig. 8.** (a) Bode plots of W after 1 h of electrode immersion in stagnant naturally aerated 0.5 M H<sub>2</sub>SO<sub>4</sub> solution at -750 mV and 25 °C. (b) Nyquist plots for W after 1 h of electrode immersion in stagnant naturally aerated 0.5 M H<sub>2</sub>SO<sub>4</sub> solution at -750 mV and 25 °C.

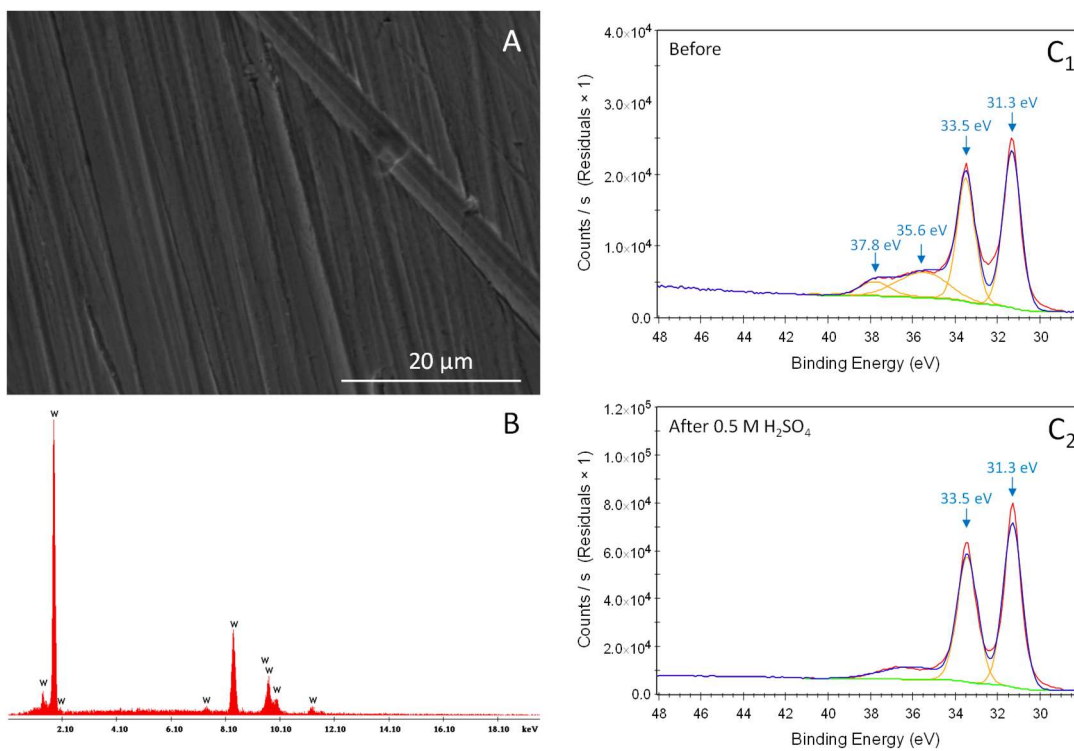


**Fig. 1.**

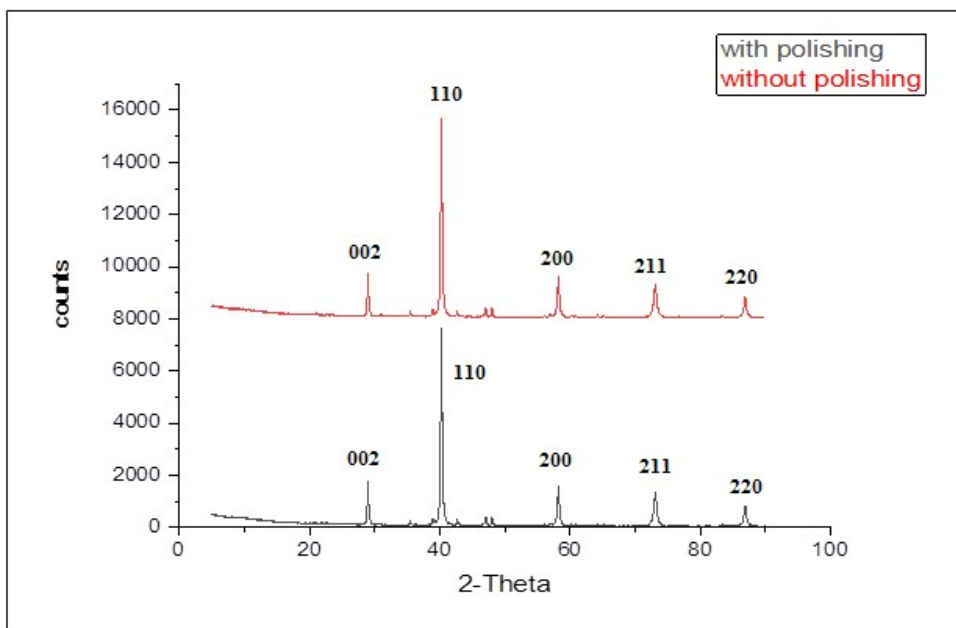


**Fig. 2.**

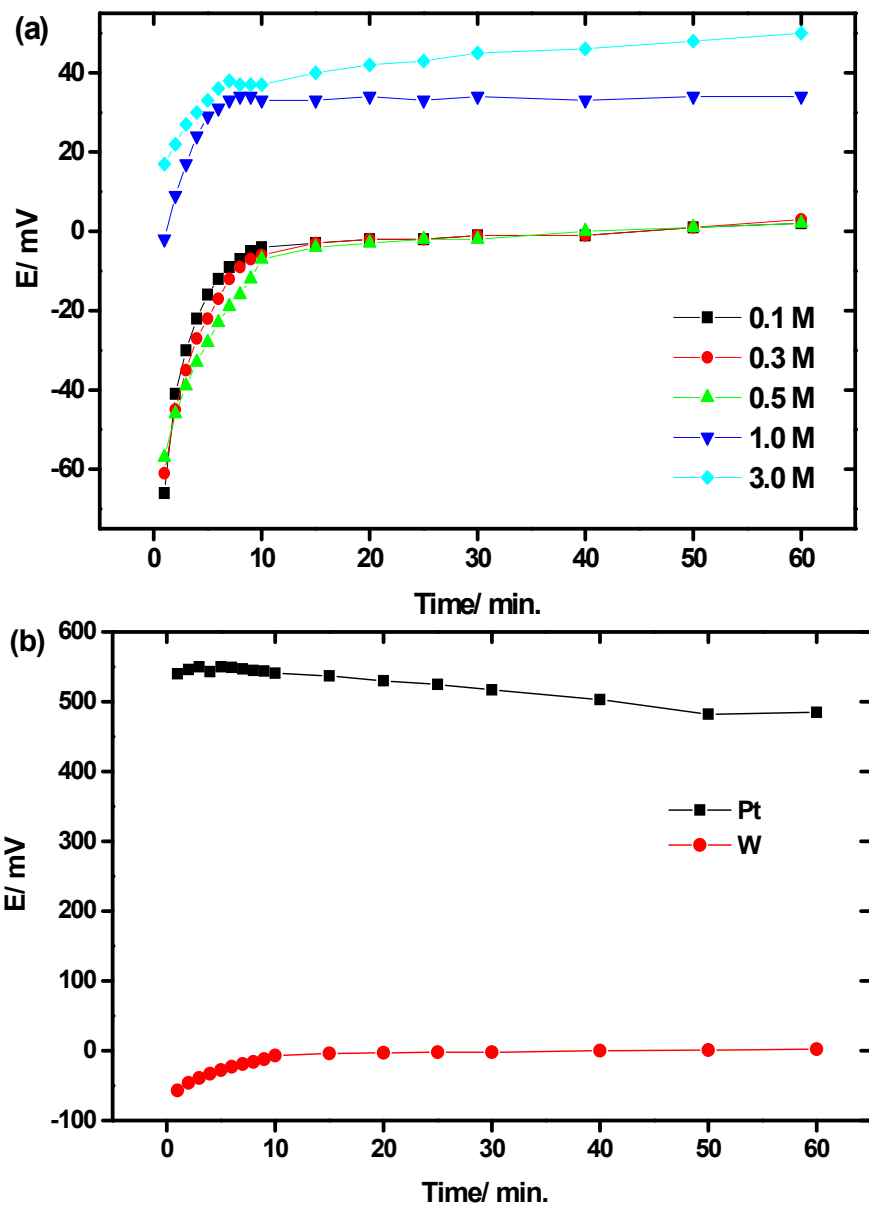


Fig. 3

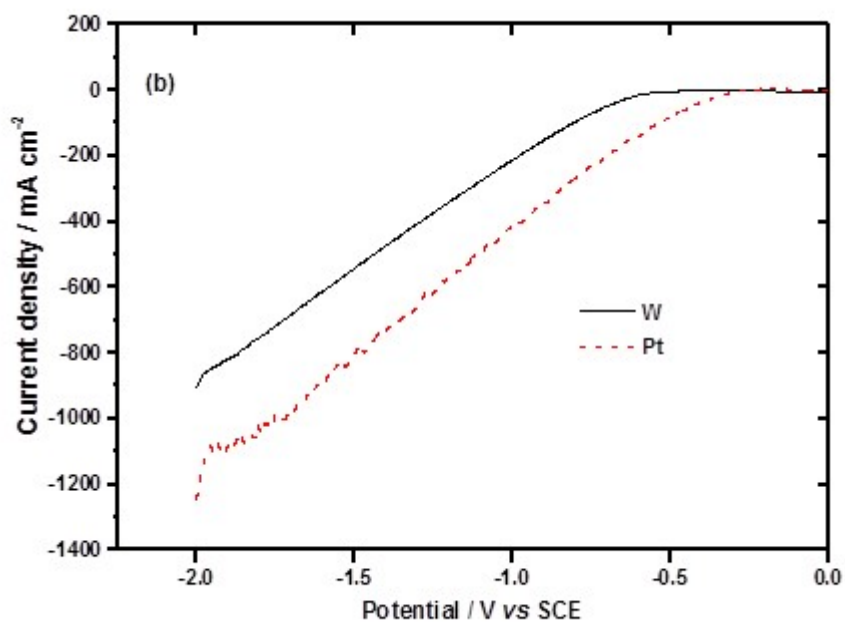
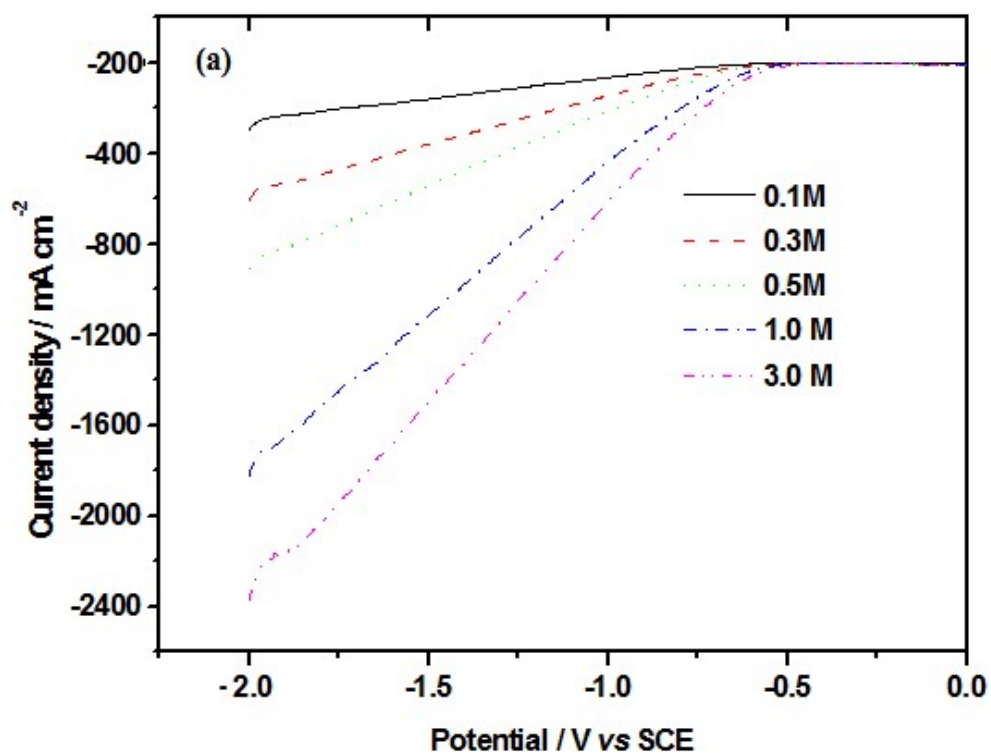


Fig. 4

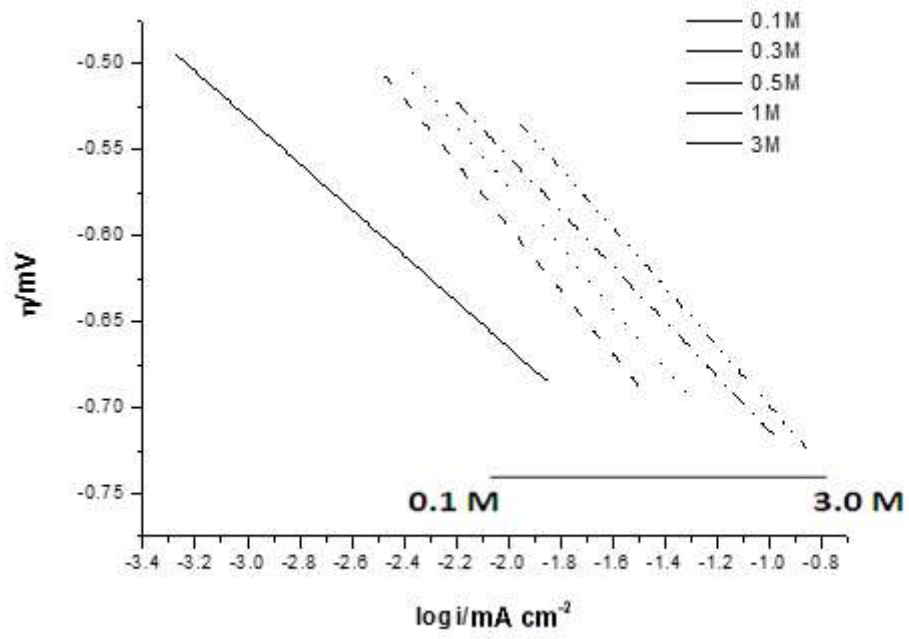


Fig. 5

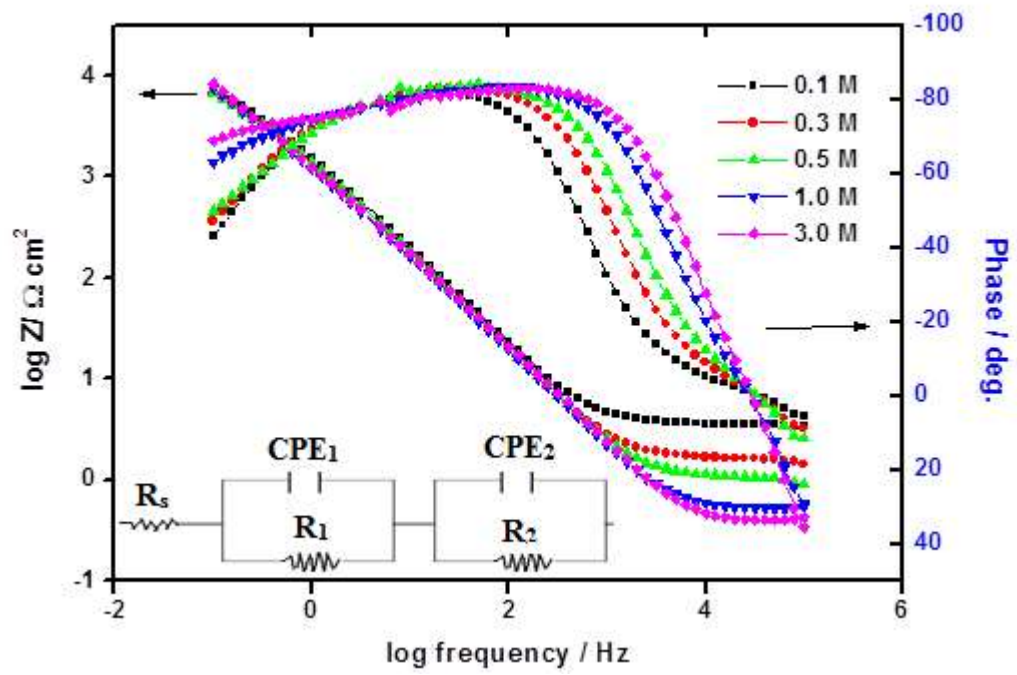


Fig. 6

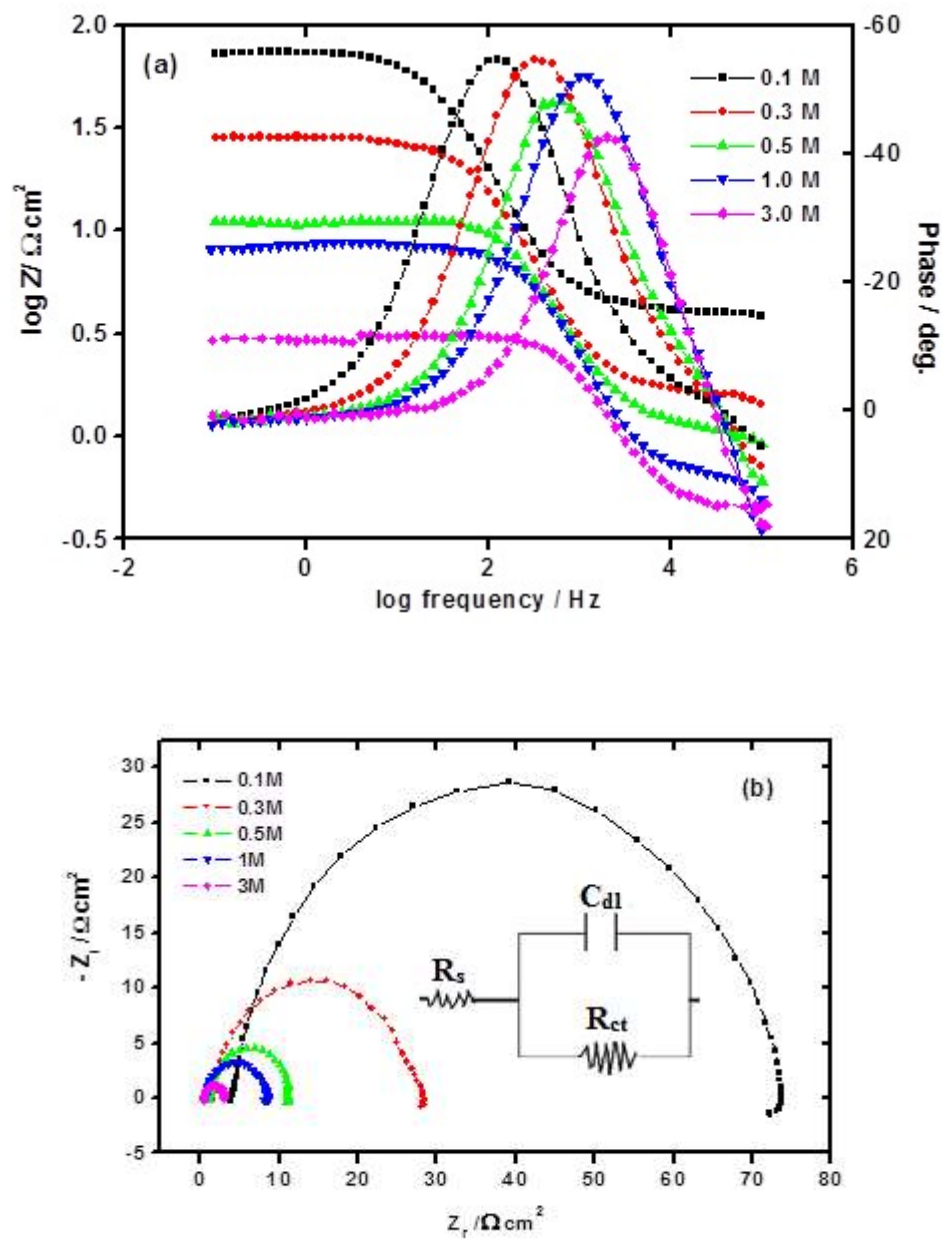


Fig. 7

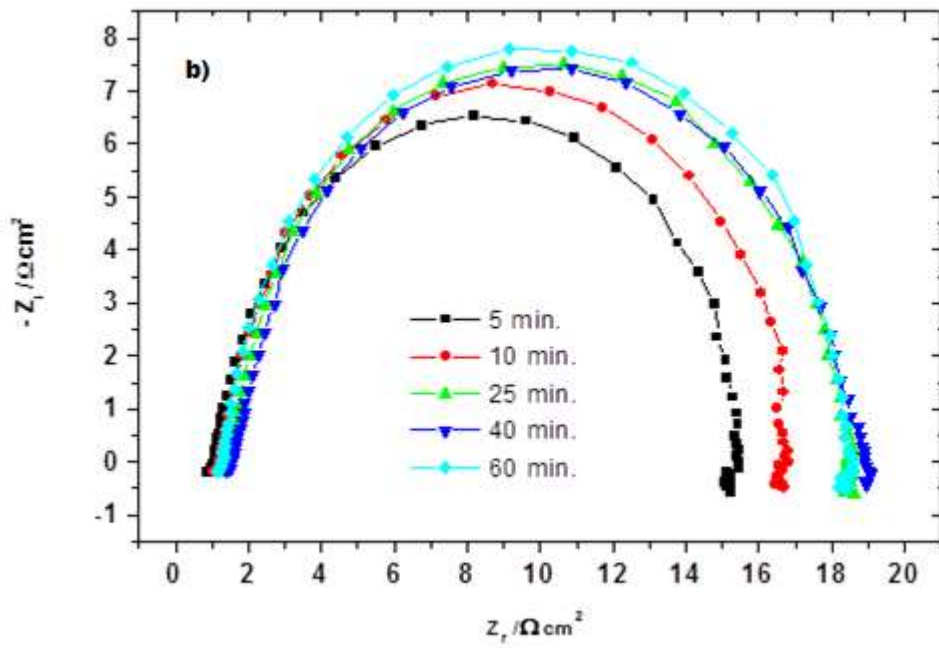
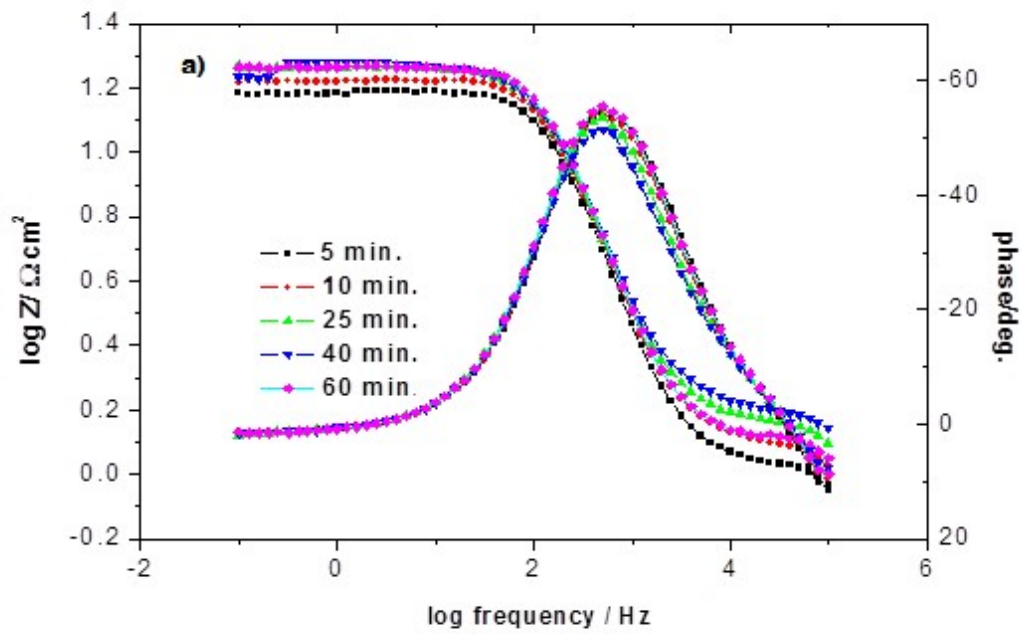


Fig. 8

## Tables

**Table 1-** Comparative performance of various HER electrocatalysts in acidic media (0.5 M H<sub>2</sub>SO<sub>4</sub>).

Electrode material	Tafel slope (mV dec <sup>-1</sup> )	Overpotential (at 10 mA/cm <sup>2</sup> ) (mV)	Reference
Core-shell MoO <sub>3</sub> -MoS <sub>2</sub> nanowires	50-60	254	[50]
MoS <sub>2</sub> nanoparticles on Au electrode	69	226	[51]
Defect-rich MoS <sub>2</sub> nanosheets	50	190	[52]
Nanostructured Ni <sub>2</sub> P	46	117	[53]
CoS <sub>2</sub>	42.4	231	[54]
CoP nanocrystals on C nanotubes	54	122	[55]
WSe <sub>2</sub> film on glassy carbon electrode	100	150	[56]
Dendritic WSe <sub>2</sub> on carbon nanofiber	80	228	[57]
WO <sub>2</sub> -carbon mesoporous nanowires	44	56	[58]
WC nanocrystals on C nanotubes	72	145	[59]
WO <sub>3</sub> (precipitated on glassy carbon)	43.9	147	[60]
WO <sub>3</sub> (annealed on glassy carbon)	39.5	73	
Pt/carbon	29	24	
MoN on N-doped C nano-octahedrons	54	62	[61]
FeSe <sub>2</sub> nanorods on graphene oxide nanosheets	64	250	[62]
Pt nanoparticles on MoS <sub>2</sub> nanosheets	52	31	[63]
	70	36	[64]
WC hybrid nanowires on carbon cloth	55	118	[65]
NiS <sub>2</sub> /MoS <sub>2</sub> on glassy carbon electrode	58-83	204-284	[66]
NiTe/NiTe <sub>2</sub> nanosheets on carbon rod	87.4	422	[67]
MoS <sub>x</sub> electrodeposited on Cu foam	43.6	200	[68]
Pt nanoparticles on N-doped carbon nanofiber	35	47	[69]
CoPS nanoparticles on N-doped carbon	68	80	[70]
Nanostructured CoP on C fiber paper	49.7	128	[71]
MoS <sub>2</sub> nanoflowers on carbon cloth	50	94	[72]
CoSe <sub>2</sub> on carbon nanotube arrays	36.7	204	[73]
Pyrazine-incorporated graphdiyne film	75	475	[74]
N-doped porous carbon	77	220	[75]
CoP <sub>2</sub> nanowire arrays on carbon cloth	67	56	[76]

Pt on porous TiN nanorod array	38.6	39.7	[77]
Polyoxometalate-encapsulated Ag-tetrazole nanocage frameworks	82	234	[78]
Pd <sub>13</sub> Cu <sub>3</sub> S <sub>7</sub> Nanoplates	49.6	64	[79]
Ni-Ni <sub>x</sub> P nanospheres on carbon cloth	76	164	[80]
AgPd alloy decorated MoS <sub>2</sub> nanosheets	82-109	215-229	[81]
Mesoporous CoS Ni P nanosheet array	45.2	41	[82]
Pd/Bi/Cu nano-architectures	61	79	[83]
Hollow Cu/Cu <sub>2</sub> O/Cu <sub>2</sub> S nanotubes	107	86	[84]
W <sub>2</sub> C nanodots on C nanotube networks	57.4	176	[85]
PtMo nanosponge wrapped with graphene dots	32	32	[86]
NiMo/NiMoO <sub>4</sub> polyhedron on Ni foam	98.9	80	[87]
W electrode	25.0	320	This work

**Table 2-** Tafel parameters for the HER on W electrode in H<sub>2</sub>SO<sub>4</sub> solution with different concentrations at 25 °C.

Conc /M	$i_0$ /mA cm <sup>-2</sup>	$-b$ /mVdec <sup>-1</sup>	$\alpha$	$1-\alpha_c$	Onset pot. / V
0.1	0.1168	0.02677	0.1668	0.8332	-0.5965
0.3	0.1182	0.02535	0.1202	0.8798	0.5874-
0.5	0.1185	0.02552	0.1258	0.8742	0.5828-
1	0.1337	0.02592	0.1395	0.8605	-0.5783
5	0.1345	0.02563	0.1296	0.8704	-0.5691

**Table 3-** Equivalent circuit parameters for W electrode measured after 1 h of electrode immersion in H<sub>2</sub>SO<sub>4</sub> solution with different concentrations at 25 °C.

Conc. /M	$R_s$ /Ω cm <sup>2</sup>	$R_T$ /kΩ cm <sup>2</sup>	$C_T$ /μF cm <sup>2</sup>
0.1	5.94	22.27	129.6
0.3	7.37	22.84	123.9
0.5	12.00	24.71	108.1
1.0	6.19	42.31	49.24
3.0	3.59	69.63	26.68

**Table 4-** Equivalent circuit parameters for W recorded after 1 h of electrode immersion in H<sub>2</sub>SO<sub>4</sub> solution of different concentration under -750 mV cathodic polarizations at 25 °C.

Conc. /M	$R_s$ /Ω cm <sup>2</sup>	$R_{ct}$ /Ω cm <sup>2</sup>	$C_{dl}$ /μFcm <sup>2</sup>
0.1	4.03	69.33	91.81
0.3	1.51	26.61	75.34
0.5	1.19	9.88	80.53
1.0	0.625	7.84	64.18
3.0	0.465	2.66	75.40

**Table 5-** Equivalent circuit parameters for W electrode measured after different intervals of electrode immersion in 0.5 M H<sub>2</sub>SO<sub>4</sub> solution under -750 mV at 25 °C.

Time /min	$R_s$ /Ω cm <sup>2</sup>	$R_{ct}$ / Ω cm <sup>2</sup>	$C_{dl}$ /μF cm <sup>2</sup>
5	1.15	14.19	70.88
10	1.31	15.37	65.44
25	1.48	16.96	75.05
40	1.58	17.26	73.75
60	1.45	13.84	72.68